Composite Structures 94 (2012) 3490–3499

Contents lists available at SciVerse ScienceDirect

Composite Structures

journal homepage: www.elsevier.com/locate/compstruct

Instantaneous delamination detection in a composite plate using a dual piezoelectric transducer network

Chul Min Yeum [a], Hoon Sohn [a,*], Jeong Beom Ihn [b], Hyung Jin Lim [a]

[a] The Department of Civil and Environmental Engineering, Korea Advanced Institute of Science and Technology, Daejeon 305-701, South Korea
[b] Boeing Research & Technology, 9725 East Marginal Way South, Mail Code 42-25 Seattle, WA 98108, United States

ARTICLE INFO

Article history:
Available online 13 June 2012

Keywords:
Delamination detection
Piezoelectric transducer network
Lamb wave
Mode decomposition
Composite structure

ABSTRACT

This study proposes a new damage detection technique so that delamination in composite plates can be detected by comparing pitch-catch Lamb wave signals obtained from a piezoelectric transducer (PZT) network without using their own baseline signals obtained from the pristine condition. The proposed technique is based on the premise that the fundamental anti-symmetric (A_0) mode slows down when it passes through a delamination area while the speed of the fundamental symmetric mode is little affected by delamination. First, the A_0 mode in each path is isolated using a mode extraction technique. This mode extraction technique is able to isolate the A_0 mode without frequency or transducer size tuning using dual PZTs composed of concentric ring and circular PZTs. Once the A_0 modes are extracted from all paths in the transducer network, the relative time delay of the A_0 mode in each path with respect to the other paths is defined as a delamination sensitive feature. Then, an instantaneous outlier analysis is developed and performed on the damage sensitive feature to identify the path(s) affected by the delaminated region(s). Because the relative time delays of the A_0 modes are instantaneously compared, robust delamination detection is achieved even under varying temperature conditions.

1. Introduction

Structural health monitoring (SHM) is a process to evaluate and assure the safety and performance of structures using data obtained from sensors. There is an increasing interest for SHM of composite aircraft as composite materials are widely used for aircraft structures. Composite materials have many advantages over metals such as lightweight and higher strength. However, composite materials are susceptible to damages such as delamination and disbond due to abrupt impact or accumulated fatigue loading. Such defects often occur beneath the surface of composite aircraft, and they are hardly visible or detectable by the naked eyes. Currently, non-destructive testing (NDT) is performed to detect such damages during ground inspections, and there are ongoing efforts to develop online SHM, which can perform automated damage diagnosis during the normal operation of aircraft.

One of such efforts is the development of an online SHM system based on Lamb wave propagation characteristics in composite structures [1–9]. In a pulse-echo mode, delamination is detected by examining waves reflected and/or scattered from the delamination [10–12]. In a pitch-catch mode, transmitted waves instead of reflected waves are analyzed for delamination detection. Similar to the pulse-echo mode, signal attenuations and time delays are commonly used features [13–17]. Furthermore, phase array transducers can be used to visualize the defect location and size. An input with a proper time delay is applied to each transducer constituting the phase array, and the phase array transducers allow steering of the principal wave propagation direction and/or focusing of propagating wave energy at desired points [18,19].

These conventional techniques often operate under the assumptions that (1) baseline signals are available from the pristine condition of the system being monitored, (2) changes from the baseline signals can be detected and related to defects, and (3) a decision boundary for damage diagnosis can also be established using the available baseline signals. However, the application of these techniques to online SHM becomes challenging, because the baseline signals are subjected to continuous changes due to continuously varying temperature and external loading conditions.

To overcome this problem, damage detection techniques which are insensitive to environmental variations have been developed by relaxing the dependency on the prior baseline signals [20–23]. The majority of work has focused on the detection of crack or corrosion damages in metallic structures. Based on polarization characteristics of piezoelectric materials, crack formation is instantaneously detected by extracting the mode conversion induced by the crack

* Corresponding author. Tel.: +82 42 350 3625; fax: +82 42 350 3610.
E-mail addresses: chulminy@gmail.com (C.M. Yeum), hoonsohn@kaist.ac.kr (H. Sohn), Jeong-Beom.Ihn@boeing.com (J.B. Ihn), limhj87@gmail.com (H.J. Lim).

0263-8223/$ - see front matter © 2012 Elsevier Ltd. All rights reserved.
http://dx.doi.org/10.1016/j.compstruct.2012.06.003

[20]. In a damage visualization technique based on phase array transducers, incident waves and additional waves backscattered from a crack are visualized and filtered to identify and locate the crack without using baseline data [21]. However, because mode conversion created by delamination is often insignificant and waves backscattered from delamination rapidly die out, the performances of the aforementioned techniques for delamination detection are less effective.

In this study, a new delamination detection technique is proposed so that delamination can be detected without using any direct comparison with previously obtained baseline data even at the presence of temperature variation. The development of the proposed technique is based on the premise that the fundamental anti-symmetric (A_0) mode slows down when it passes through a delamination area while the speed of the fundamental symmetric (S_0) mode is little affected by delamination. Based on this assumption, the existence of delamination can be detected by comparing the time delay of the A_0 mode in each path with respect to the other paths in the transducer network rather than with the previously obtained baseline data. For the extraction of the A_0 mode in each path, a mode extraction technique using dual PZTs, which are composed of ring and circular PZTs, is proposed. Once the relative time delays of the A_0 modes are computed from all the paths in the transducer network, an instantaneous outlier analysis is conducted so that the path(s) crossing the delamination area can be automatically identified using only current data. The effectiveness of the proposed technique is experimentally validated under varying temperature conditions using a simple composite plate and a composite specimen with stiffeners. The uniquenesses of this study lie in that (1) robust delamination diagnosis can be achieved even under varying temperature, (2) multiple delaminations can be detected, and (3) the proposed technique can be also applied to complex structures.

This paper is organized as follows. In Section 2, the effects of delamination and temperature on Lamb wave modes are investigated. In Sections 3 and 4, the mode extraction and delamination detection algorithm are proposed, respectively. The applicability of the proposed technique to delamination detection in simple and complex composite structures is investigated in Sections 5 and 6, and followed by the conclusion in Section 7.

2. The effects of delamination and temperature on Lamb wave modes

In this section, the effects of delamination and temperature on Lamb wave propagation are compared to justify the development of the proposed damage detection technique under temperature variation. Here, only a brief summary of the numerical and experimental studies conducted is presented. Note that the pitch-catch Lamb wave signals presented in Fig. 1 are obtained from the composite plate presented in Section 5, and the experimental details are provided in Section 5. The findings are summarized as below.

(1) Fig. 1a shows that the A_0 mode slows down when it passes through a delamination area while the speed of the S_0 mode does not change much at delamination. Furthermore, a proportional relationship between the severity of delamination and the time delay of the A_0 mode is observed.
(2) As delamination increases, the amplitude of the A_0 mode is slightly amplified initially and followed by attenuation with a further increase of delamination. A similar initial amplification of the A_0 mode is also reported by others [15].
(3) A numerical simulation also reveals that the A_0 mode is more significantly delayed and attenuated by delamination than the S_0 mode. This is because delamination primarily decreases interlaminar shear strength, and the A_0 mode is dominantly affected by the shear modulus of the specimen.
(4) Mode conversion occurs due to delamination, but the converted modes rapidly attenuate, making it difficult to reliably measure the converted modes. The numerical simulation shows that the amplitude of the converted modes due to delamination is typically less than 1% of the amplitudes of the A_0 and S_0 modes.
(5) The waveforms of the A_0 and S_0 modes are hardly distorted by delamination because the frequency content of the propagating waves is little affected by delamination.

Next, the effect of temperature is investigated. Similar to the effect of delamination, the amplitude and arrival time of the A_0 mode are affected by temperature variation. More specifically, Fig. 1b shows that, as temperature increases, the A_0 mode amplitude decreases and the arrival time of the A_0 mode is delayed. However, the S_0 mode characteristics are rarely affected by temperature. Note that, the second wave packet in the Fig. 1 is, in fact, the superposition of the first arrival A_0 mode and the S_0 modes reflected from structural boundaries. Because the S_0 mode characteristics are not much affected by either delamination or temperature variation, it can be assumed that the variation of the second wave packet is mainly due to the influence of the temperature and delamination on the first arrival A_0 mode not on the reflected S_0 modes.

These observations reveal the challenge of applying the conventional damage detection techniques to in-flight aircraft. Because of the similarity of the delamination and temperature effects on Lamb wave modes, it is difficult to infer the damage state of aircraft simply by comparing the current data with the baseline data under varying temperature conditions. To address this issue, a reference-free technique, which does not rely on previously obtained baseline data, is developed for robust delamination detection in

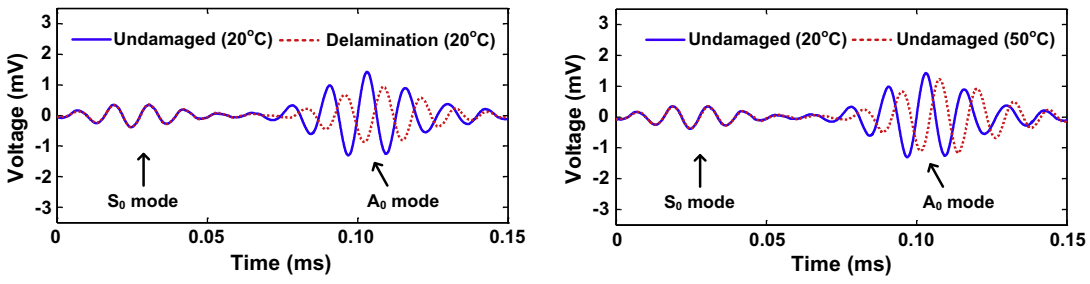

(a) Delamination effect (b) Temperature effect

Fig. 1. The investigation of the effects of delamination and temperature on Lamb wave propagation based on experimental data obtained from the composite specimen test: Both described in Section 5: delamination and temperature mainly cause time delay and attenuation of the A_0 mode.

multi-layer composite materials under temperature variation. Since the proposed technique relies on the time delay of the A_0 mode due to delamination, it is necessary to isolate the A_0 mode from measured pitch-catch signals. In the next section, a mode extraction technique, which can isolate the A_0 mode, is introduced.

3. Lamb wave mode extraction technique

The proposed mode extraction technique isolates only the A_0 mode by scaling two Lamb wave signals, which are obtained from the same path but with two different sensing PZT sizes. The measurement of such signals from the same path with different sizes is made possible using a specially designed PZT transducer called a dual PZT, which is composed of collocated inner circular and outer ring PZTs. Note that the proposed technique is an extension of the previous one proposed by the authors [24].

The advantages of the proposed mode extraction technique are that (1) PZTs need to be placed only a single surface of a structure, (2) mode extraction can be performed at any desired frequency without physical adjustment of the PZT size and/or spacing, and (3) the circular design of the dual PZT allows the extraction of the A_0 modes from Lamb wave signals propagating in any directions.

3.1. Descriptions of the dual PZT and signal notations

The schematic drawing of a dual PZT, which is used for the A_0 mode extraction, is shown in Fig. 2a. The dual PZT is composed of concentric inner circular and outer ring PZTs, which can be selectively activated for actuation and sensing [22,25]. By activating the ring and circular parts of the excitation and sensing dual PZTs either independently or simultaneously, nine different signal combinations can be obtained from a pair of dual PZTs. For simplicity, the concept of the proposed technique is described using only two signal components, V_{rr} and V_{rc}. V_{rr} denotes a response measured by the ring portion of the sensing dual PZT, when the outer ring of the exciting PZT is used for excitation. Similarly, V_{rc} is obtained by the inner circular component of the sensing dual PZT for the same exterior ring excitation. The darker (red) areas in Fig. 2b show the PZT parts activated for either Lamb wave excitation or sensing.

3.2. A theoretical Lamb wave propagation model using circular PZTs

The proposed mode extraction technique is formulated based on a 3D Lamb wave propagation model between a pair of circular actuation and sensing PZTs. One pair of circular PZTs mounted on the surface of an isotropic structure is used as an actuator and a sensor in a pitch-catch mode. The PZT actuation is modeled as an in-plane traction force along its free edge, and the PZT response is computed by integrating the strain over the sensing PZT area [24]. Eq. (1) shows the output voltage response at time t, $V(t)$, obtained from the circular sensing PZT with a radius of c when another circular PZT with a radius of a is used as an actuator. The details of Eq. (1) is provided in Appendix A.

$$V(t) = C^{S_0}(t, r_s) S^{S_0}(a, c) + C^{A_0}(t, r_s) S^{A_0}(a, c) \tag{1}$$

$$\text{where } C^{S_0}(t, r_s) = -i \frac{2\sqrt{2\pi}\tau_0 E_s h_s g_{31}}{\mu \sqrt{\xi^{S_0} r_s}} \frac{N_S(\xi^{S_0})}{D'_S(\xi^{S_0})} e^{i\left(\omega t - \frac{\pi}{4} + \xi^{S_0} r_s\right)},$$

$$C^{A_0}(t, r_s) = -i = -i \frac{2\sqrt{2\pi}\tau_0 E_s h_s g_{31}}{\mu \sqrt{\xi^{A_0} r_s}} \frac{N_A(\xi^{A_0})}{D'_A(\xi^{A_0})} e^{i\left(\omega t - \frac{\pi}{4} + \xi^{A_0} r_s\right)},$$

$$S^{S_0}(a, c) = \frac{a}{c} J_1(\xi^{S_0} a) J_1(\xi^{S_0} c), S^{A_0}(a, c) = \frac{a}{c} J_1(\xi^{A_0} a) J_1(\xi^{A_0} c).$$

The derived Lamb wave propagation model in Eq. (1) reveals three key features, which are necessary for the development of the proposed mode extraction technique: (1) The Lamb wave modes measured and/or excited at different sizes of the PZTs have identical arrival times but different amplitudes. The arrival times of the S_0 and A_0 modes are controlled only by the distance between the sensing and excitation PZTs (r_s) and not affected by their sizes (a and c). On the other hand, the amplitudes of the S_0 and A_0 modes are functions of the PZT sizes. (2) The amplitudes of the S_0 and A_0 modes change at "different" rates, as the sizes of the exciting and/or sensing PZTs vary. Because the Bessel functions in Eq. (1) are not linear functions with respect to the PZT sizes, the amplitude change rates of the S_0 and A_0 modes are not identical as the sizes of exciting and/or sensing PZTs vary. (3) The amplitude change rate of each mode is independent of the wave propagation distance because it only depends on the PZT sizes and a wavenumber of the corresponding mode.

3.3. Procedure for the proposed mode extraction technique

Based on three key features discussed in the previous subsection, the two signals V_{rr} and V_{rc} obtained from a pair of dual PZTs satisfy the following conditions: (1) The S_0 and A_0 modes in V_{rr} and V_{rc} have an identical arrival time but different amplitudes. (2) The amplitude ratio of the S_0 mode in V_{rr} to that in V_{rc}, denoted as S_c, is different from the amplitude ratio of the A_0 mode in V_{rr} to that in V_{rc}, denoted as A_c. (3) S_c remains constant regardless whether the amplitude of the S_0 mode is taken from the first

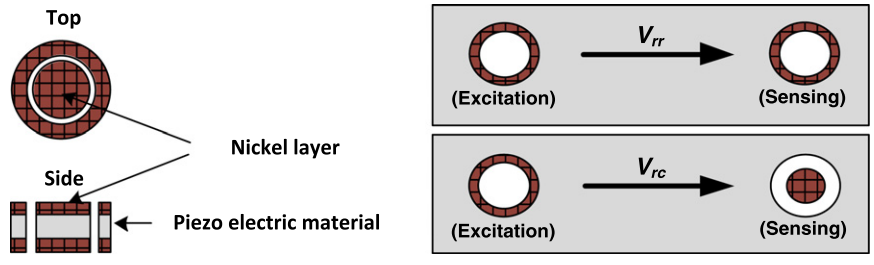

(a) A schematic drawing of the dual PZT

(b) Notations of signals

Fig. 2. A schematic drawing of the dual PZT and examples of signals obtained by the dual PZTs: V_{rr} denotes a response measured by the ring portion of the sensing dual PZT, when the outer ring of the exciting PZT is used for excitation. Similarly, V_{rc} is obtained by the inner circular component of the sensing dual PZT for the same exterior ring excitation. The darker (red) area of the dual PZT represents the PZT component activated either for excitation or sensing. (For interpretation of the references to colour in this figure legend, the reader is referred to the web version of this article.)

arrival, reflected, or overlapped signals. Thus, since S_c is not identical to A_c, the A_0 mode can be extracted by simply scaling one of V_{rr} and V_{rc} with respect to the other so that the S_0 modes in both signals can have the same amplitude.

The proposed mode extraction technique is illustrated in Fig. 3 using V_{rr} and V_{rc} obtained from one of dual PZT pairs placed on the test specimen in Fig. 5. The procedure of the proposed mode extraction technique can be summarized as follows:

(1) In a pitch-catch mode, V_{rr} and V_{rc} are measured by the ring and circular parts of the sensing dual PZT when the ring part of the exciting dual PZT is actuated as shown in Fig. 3a.
(2) One out of V_{rr} and V_{rc} is scaled so that the S_0 modes in both signals have the same amplitude (Fig. 3b).
(3) By subtracting scaled V_{rc} from V_{rr}, all the S_0 modes including the first arrival and reflections are removed and the only A_0 mode remains as shown in Fig. 3c.
(4) A matching pursuit technique is further employed to remove unwanted error for the proposed mode extraction technique in Fig. 3d. (The detail of this step is explained in Section 3.4.)

Here, the pair of V_{rr} and V_{rc}, is used to demonstrate the mode extraction technique. In practice, any pair of two pitch-catch signals can be used as long as they are measured or excited by two different parts of dual PZT transducers. Note that this study only concern about the arrival time of the first arrival A_0 mode not the amplitude information, and that's what is exactly provided by the presented mode extraction technique. In addition, the proposed technique can be effectively applied to the wave propagation path(s) with delamination as long as the attenuation and distortion of the S_0 mode are negligible as shown in Fig. 1a.

3.4. Signal filtering using a matching pursuit technique

There are two primary sources of error for the proposed mode extraction technique: the spreading error and the varying material properties depending on the wave propagation direction in anisotropic composite plates [24]. The spreading error stems from the fact that V_{rr} and V_{rc} are measured by two co-centered PZTs with different sizes. When a specific Lamb wave mode is measured by a sensing PZT, the propagating wave packet hits the front side of the sensing PZT first and exits from its tail. Therefore, the larger the sensing PZT is, the more spread out the PZT response, which is the strain averaged over the entire area of the sensing PZT, is in the time domain. However, the arrival time of propagating wave packets are still the same regardless of the sensing PZT size as discussed in Eq. (1). The spreading error appears in the extracted signal when V_{rr} and V_{rc} are subtracted from each other after scaling.

Another type of error results from the fact that the material properties of an anisotropic composite plate vary depending on the wave propagation direction. That is, the first arrival S_0 mode and other subsequent S_0 modes reflected from boundaries will have different wavenumbers because they propagate in different directions. This can be translated to the fact that S_c is not constant throughout the signal, producing errors in the extracted signal.

These two types of error make it difficult to fully remove the S_0 modes from V_{rr} and V_{rc} because (1) waveforms of the S_0 modes in scaled V_{rc} and V_{rr} are not exactly matched due to the spreading error and (2) the S_c estimated from the first arrival S_0 mode is not the same as those from the other S_0 modes reflected from boundaries. Fig. 3c shows that the S_0 modes with small amplitudes still remain in the extracted signal in step (3) and are overlapped with the A_0 mode.

To tackle this issue, a matching pursuit technique is applied in the last step of the mode extraction procedure [26–28]. The matching pursuit technique is a signal processing technique that iteratively decomposes a target time signal into a linear combination of basic functions. At the first iteration, parameters of the first basis function, such as arrival time, scale, amplitude, are optimized so that the target signal can be best projected on to the first basis function. Next, the residual signal, which is the remaining component of the target signal after projected onto the first basis function, is now projected onto the second basis function. Finally, these steps are repeated until all wave components of interest are identified and decomposed. Since the A_0 mode is the only dominant mode of interest in the extracted signal in step (3), only one iteration of the matching pursuit is performed to extract the A_0 mode in this study. The matching pursuit technique is

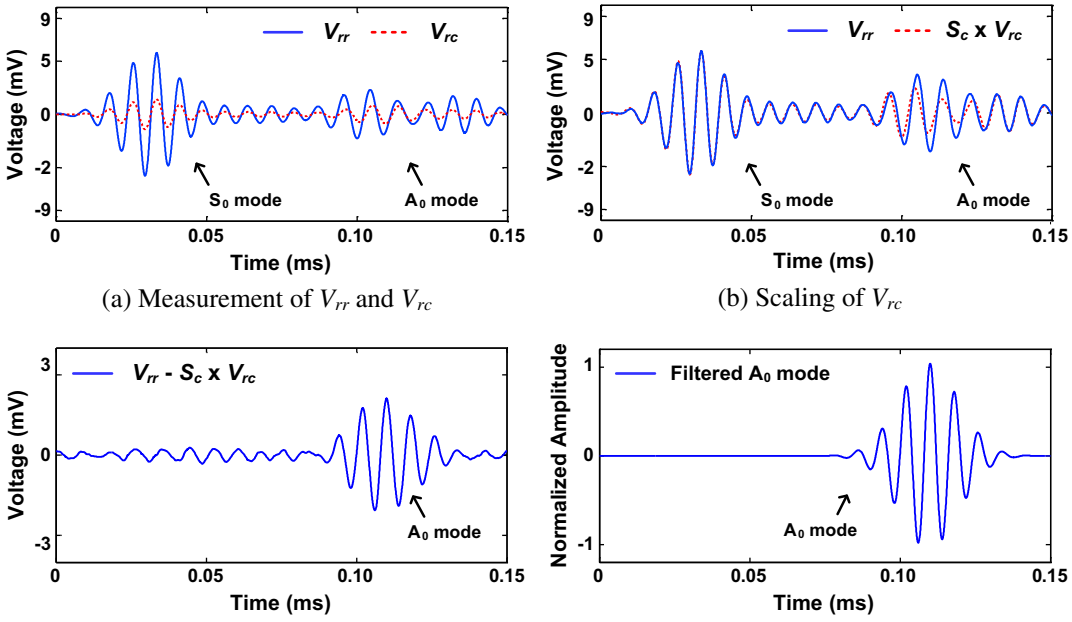

(a) Measurement of V_{rr} and V_{rc}

(b) Scaling of V_{rc}

(c) Extraction of the A_0 mode

(d) Filtered the A_0 mode using a matching pursuit technique

Fig. 3. Illustration of the A_0 mode extraction using the proposed mode extraction technique.

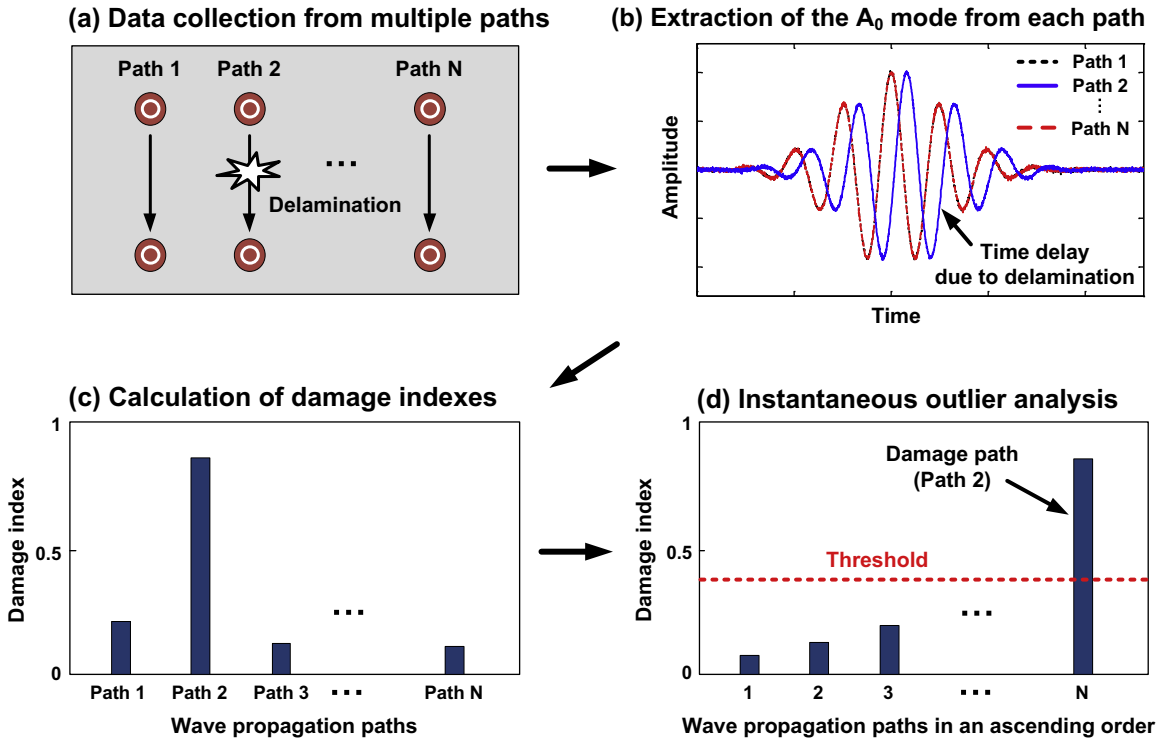

Fig. 4. Overview of the proposed instantaneous delamination detection technique: (a) collect pitch-catch Lamb wave signals from the dual PZT network, (b) extract the A_0 modes from all the wave propagation paths using the proposed mode extraction technique, (c) calculate the damage index, which is indicative of the time delay of the A_0 mode with respect to the other paths, and (d) identify the wave propagation paths affected by delamination using an instantaneous outlier analysis.

advantageous because (1) only the A_0 mode can be extracted from a signal including unwanted S_0 modes, which cannot be not fully canceled in the mode extraction process, and (2) the measurement noise included in a signal can be effectively filtered out by reconstructing the A_0 mode waveform. More detailed discussion on the matching pursuit technique can be found [26].

4. Instantaneous delamination detection technique

In this section, the necessary steps for the proposed instantaneous delamination technique are described. The proposed technique is named as "instantaneous" because damage diagnosis is performed by comparing multiple pitch-catch signals instantaneously obtained from a dual PZT network and it does not relying on the 'baseline' data collected from the past undamaged conditions. In this way, susceptibility to false alarms due to operational and environmental variations of a structure is minimized [29].

The overview of the proposed delamination detection technique is shown in Fig. 4. First, pitch-catch Lamb wave signals are obtained from multiple actuator–sensor combinations in the dual PZT network. Second, the first arrival of the A_0 mode is extracted from all signals in the dual PZT network using the proposed mode extraction technique. Third, a damage index, which indicates the relative time delay of the A_0 mode in the specific path with respect to the other paths, is computed. Finally, when the damage index of a specific path becomes significantly larger than these of the other paths, the proposed instantaneous outlier analysis diagnoses that delamination is along the specific path.

4.1. Data collection from the dual PZT transducer network

An array of PZTs is installed on the composite structure for delamination detection and localization. Each PZT acts as both an actuator and a sensor for Lamb wave excitation and sensing. One PZT is designated as an actuator, exerting a predefined toneburst waveform into the structure. Then, the adjacent PZTs measure the corresponding response signals. This pitch-catch process is repeated for all the wave propagation paths available. Then, the wave propagation paths are divided into groups composed of the paths having the same wave propagation distance and direction for the later computation of the damage index.

4.2. Extraction of the A_0 mode from each path

Note that multiple reflections from structural boundaries and geometric features like stringers can overlap with the target A_0 mode, making the isolation of the A_0 mode challenging. In particular, this overlapping is more likely a problem in composite structures because the difference between S_0 and A_0 mode group velocities is larger in composite structures than in metallic structures. In such cases, the A_0 mode is extracted from each path using the mode extraction technique described in Section 3 before proceeding to the next step.

4.3. Calculation of the damage index

Once the A_0 modes are identified from all the paths, a damage index of the ith path, DI(i), is defined to examine how much the A_0 mode in the ith path is delayed compared with the A_0 modes in the other paths. The basic assumption for the calculation of the proposed damage index (DI) is that more than half of the paths in the same group, which consists of the paths having the same wave propagation distance and direction, are collected from the undamaged condition. In other words, it is assumed that damage is localized and only a few paths are affected by delamination.

$$\mathrm{DI}(i) = \frac{1}{N_f}\sum_{f}^{N_f}\frac{1}{2}\left\{1 - \frac{1}{\alpha}\sum_{j}^{\alpha} corr(A_0(f,i), A_0(f,j))\right\} \tag{2}$$

where *corr* is the cross-correlation operator, f is the excitation frequency, and A_0 (f,i) denotes the first arrival A_0 mode of the ith path measured at f. It is assumed that at least half of all the paths available in each group are collected from the undamaged conditions, and the group velocities of these paths correspond to the first half of the fastest A_0 modes in the group. Then, α is set to be the number of the assumed undamaged paths in each group. The DI value is averaged over N_f different frequencies and normalized so that its value falls within 0–1. A larger DI value indicates a higher probability of delamination within the corresponding path.

4.4. Instantaneous outlier analysis

An outlier analysis is performed on the DIs to identify the path(s) affected by delamination. A common practice for such decision making has been to collect damage sensitive features from the baseline condition of a structure, characterize the distribution of the features, and establish a threshold value corresponding to a user-specified confidence level. If any specific feature value exceeds the threshold, the corresponding path is defined as damaged. However, the threshold value predetermined from the baseline data may falsely indicate damage or allow damage to go undetected at the presence of varying environmental conditions.

In this study, an instantaneous outlier analysis with an adaptive threshold value is proposed to automatically detect damaged path(s) among all the available wave propagation paths in the PZT network. The procedure of the proposed instantaneous outlier analysis can be summarized as follows.

(1) Calculate the DI, which indicates the time delay of the A_0 mode, for all the available paths in the PZT network.
(2) Arrange the entire DIs in an ascending order (1st index: the smallest and Nth index: the largest).
(3) Fit a parametric distribution function to the $n-1$ smallest DIs, and compute a threshold corresponding to a user specified confidence level. Here, the initial n is selected typically to be the half of the available path number.
(4) If the value of the nth smallest DI is larger than the threshold value, the PZT paths associated with the nth, n + 1st…Nth indices are determined to be damaged. If not, repeat steps (3) and (4) for the next smallest value $(n+1)$ until n reaches N.

Because the range of the DI is limited from 0 to 1, a truncated exponential distribution is used for the parametric estimation of the DI distribution. The truncated exponential distribution with a parameter c has the following probability density function [30]:

$$P(x) = ce^{-cx}(1-e^{-c})^{-1}, \quad (0 < x \le 1) \tag{3}$$

Here, x denotes DIs obtained from paths. The parameter c can be obtained from the maximum likelihood estimator, c_b, as follows.

$$\bar{x} = 1/c_b - 1/(e^{c_b} - 1) \tag{4}$$

where $\bar{x}$ is the mean of x.

5. Delamination detection in a composite plate specimen

5.1. Description of the experimental set-up

To validate the proposed delamination detection technique, a multi-layer carbon fiber composite plate shown in Fig. 5a is tested. The material properties and prepreg lay-up information of the specimen are unknown to the authors. The dimensions of the specimen are 1512 mm × 762 mm × 5 mm, and 9 dual PZTs are installed on the inside surface of the specimen in a square grid pattern with 150 mm spacing using a high-strength adhesive. Each dual PZT is composed of inner circular and outer ring PZTs, and the radius of the circular PZT, and the radii of the inner and outer rings of the exterior ring PZT are 2 mm, 3 mm and 4 mm, respectively. The dual PZT is packed by a Teflon layer for insulation and protection, and printed copper wires and SMA connectors are used for easy installation [25]. Each dual PZT acts as either an actuator or a sensor for Lamb wave excitation and sensing. A total of 20 pitch-catch signals are obtained from the 9 dual PZTs and divided into four different groups having the same wave propagation distance and direction. For example, "group 1" in Fig. 5b contains four vertical paths with 150 mm spacing. Note that the other groups, which include longer paths such as 2–7 or 2–3 paths (here, the first and second numbers indicate the numbers of excitation and sensing PZTs), are excluded in this test due to the limited number of the paths in each group.

A conventional drop-weight impact tester with a 10 mm radius steel ball tip is used to introduce low velocity impact damage. Three consecutive impacts are applied to a single point, exerting 24.5 J energy each time. In this manner, delaminations are sequentially formed at three locations: (1) Damage 1 in the middle of 4–3 path, (2) Damage 2 in the middle of 2–5 path, and (3) Damage 3 at the intersection of 2–4 and 1–5 paths, respectively.

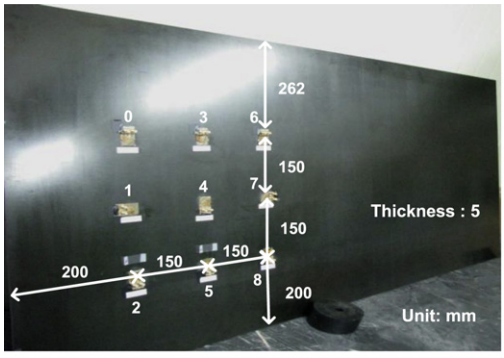

(a) A layout of the dual PZT network

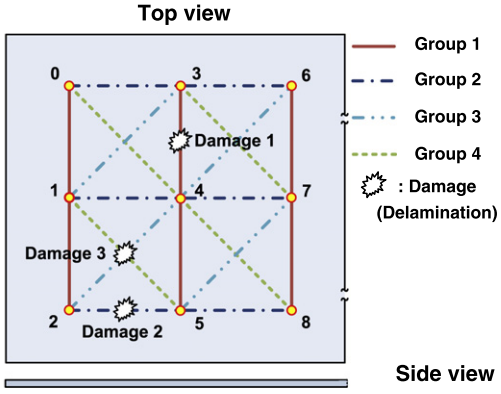

(b) Damage locations and wave propagation paths

Fig. 5. A composite plate specimen with a surface mounted PZT transducer network: for the calculation of the DI in Eq. (2), pitch-catch signals are obtained from a total of the 20 paths, and they are divided into four different groups having the same wave propagation distance and direction.

Fig. 6 shows the data acquisition system and temperature chamber used in this study. The data acquisition system consists of an arbitrary waveform generator (AWG), a high speed signal digitizer (DIG), a low noise preamplifier (LNP), a high power amplifier and eight multiplexers. A 7 cycle toneburst signal with a 10 peak-to-peak voltage is generated using the 14-bit AWG, amplified by a power amplifier with a gain of three, and then applied to the PZT. The voltage PZT response is filtered and amplified 50 times by the LNP and measured by the 16-bit DIG with a sampling rate of 20 MS/s. The response signals are measured 20 times and averaged in the time domain to improve the signal-to-noise ratio. Frequency sweeping is performed from 80 kHz to 120 kHz with a 10 kHz interval. The frequency band is selected to be below the cutoff frequencies of the A_1 and S_1 modes, and the A_0 mode is more dominant than the S_0 mode within this frequency band. For each delamination condition, temperature chamber experiments are conducted at −10, 20 and 50 °C, respectively.

5.2. Test results

The effects of temperature and delamination on Lamb wave modes are investigated in Fig. 1. Lamb wave signals used in Fig. 1 are obtained from path 4–3 on the specimen at an input frequency of 100 kHz. By comparing Lamb wave signals measured from the undamaged and delamination conditions, it is observed that the A_0 mode slows down and attenuates when it passes through a delamination area. Similarly, the A_0 mode is attenuated and delayed as temperature increases. However, the S_0 mode does not change much due to either delamination or temperature variation.

Fig. 7 shows how the arrival time of the A_0 mode in path 4–3 changes with respect to those in the other vertical paths within the group 1 when delamination is introduced in the middle of path 4–3. All signals are obtained at 50 °C. Fig. 7a shows that the A_0 mode in path 4–3 is not delayed compared with the others. However, when delamination is introduced in the middle of path 4–3, a clear time delay of the A_0 mode in path 4–3 (a solid blue[1] line) is observed in Fig. 7b.

Fig. 8 illustrates the proposed instantaneous outlier analysis. The damage indexes in Fig. 8a and b are obtained from the intact and damaged conditions of the plate at 50 °C, respectively. In each figure, a pair of two numbers with an arrow identifies the test path, and the number in the abscissa axis represents the order of the test path when all the paths are sorted in an ascending order. For example, "1–5" and "11" in the very left subfigure in Fig. 8a indicates that the wave propagation path obtained by exciting PZT 1 and measured by PZT 5 has the 11th smallest DI value, and this path is currently being tested using the instantaneous outlier analysis. At this point, the threshold (a solid red line) is determined by fitting a truncated exponential distribution to the $n-1$ smallest DI, and computing a one-sided 99.9% confidence interval. The outlier analysis started with the 11th smallest DI value, assuming that the first half of the sorted DI values ($n = 20/2$) does not correspond to damaged paths. If the DI value of the test path becomes larger than the corresponding threshold value, the remaining paths having higher DI values are determined to be damaged including the test path. If not, the process continues with the next smallest DI value until it reaches the largest DI. In Fig. 8a, because the DI of each test path is smaller than the corresponding threshold value, it is concluded that there is no delamination in the test plate. In Fig. 8b, the 16th smallest DI value becomes larger than the threshold, indicating that the paths corresponding to this DI and the larger DI values pass through the delamination.

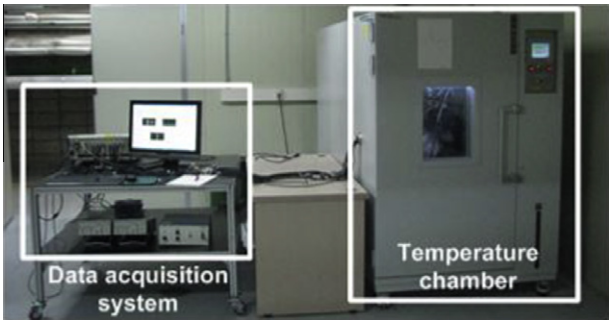

Fig. 6. The data acquisition system used for Lamb wave excitation and sensing, and a temperature chamber used for varying temperature experiments.

The test results under three different temperatures (−10, 20 and 50 °C) are summarized in Table 1 for the intact and three damage cases. For the intact case, no false-positive alarm was produced, and all damaged paths are successfully detected for the damage cases. In addition, a goodness-of-fit test using the Kolmogorov–Smirnov (K–S) test [31] has confirmed that the truncated exponential distribution properly describes the population of the DI values obtained from the intact and all damage cases.

6. Delamination detection in a complex composite specimen with stiffeners

6.1. Description of the experimental set-up

Next, a composite specimen with three co-cured hat-shape stiffeners shown in Fig. 9a is tested. The material properties and prepreg lay-up information of the specimen are not provided to the authors. The dimensions of the specimen are 760 mm × 460 mm × 10 mm, and the dimensions of the upper width, lower width, thickness and height of the hat-shaped stiffener (from the plate to the upper part of the stiffener) are 25 mm, 70 mm, 3 mm and 30 mm, respectively. Ten dual PZTs are installed across the center stiffener in a rectangular grid pattern with 210 mm horizontal and 80 mm vertical spacing. The radius of the circular PZT and the radii of the inner and outer parts of the ring PZT are 3 mm, 4 mm and 7 mm, respectively. The dual PZT used in this experiment is fabricated by etching the top nickel electrode layer of a PZT into outer and inner parts [25]. Fig. 9b shows a total of 17 pitch-catch signals are obtained from the 10 dual PZTs and divided into 3 different groups having the same wave propagation distance. Since the specimen exhibits transverse isotropic behavior in 45° and 135° directions, the paths in these two directions are merged into a single group.

A nitrogen gas gun with a 2.5 mm radius steel ball is used to introduce high velocity impact damage on the specimen. Due to the special materials used in this study and its thickness (10 mm), repeated high-velocity impacts are necessary to seed delamination. Five consecutive impacts are applied to a single point, exerting 180 J energy each time. In this manner, delamination is formed at a crossing point between 4–7 and 5–6 paths, which is located under the second hat-shaped stiffener.

Because of the increased thickness of the specimen compared to the previous specimen, frequency sweeping is performed from 40 kHz to 50 kHz with a 2 kHz interval instead of 80 kHz to 120 kHz with a 10 kHz interval. The rest of the test configuration is identical to the previous test.

[1] For interpretation of color in Figs. 1–10, the reader is referred to the web version of this article.

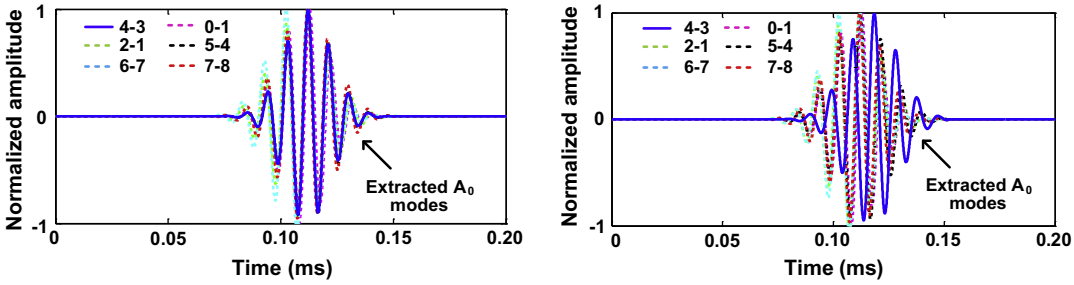

(a) No damage (Case 1 in Table1) (b) Damage 1 (Case 2 in Table 1)

Fig. 7. Comparison of the A_0 modes obtained from 'No damage' and 'Damage 1' cases. The A_0 modes are extracted from six vertical paths within group 1 shown in Fig. 5. Delamination is placed in the middle of path 4–3 (a solid blue line). (For interpretation of the references to colour in this figure legend, the reader is referred to the web version of this article.)

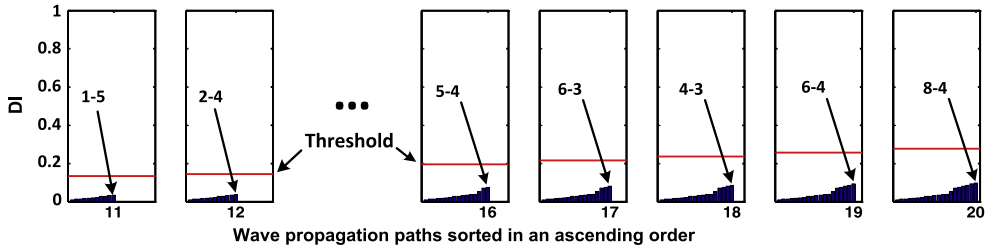

(a) No damage (Case 1 in Table 1)

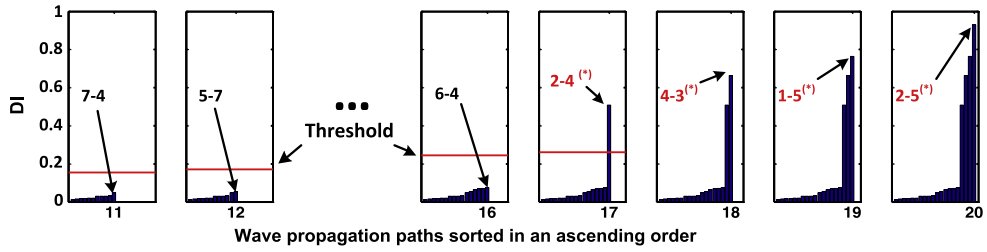

(b) Damages 1, 2 and 3 (Case 4 in Table 1. '*' is the detected damaged paths.)

Fig. 8. Examples of the instantaneous outlier analysis using an automatically determined threshold. The threshold is continuously updated until the DI of the test path becomes larger than the corresponding threshold or the outlier analysis reaches the largest DI value.

Table 1
Instantaneous diagnosis under changing temperatures (a composite plate).

Case	Damage location	Temp. (°C)	Threshold value	Damaged path(s) (DI value)	Damage diagnosis
1	No damage	−10	0.164	None	No damaged path detected
		20	0.247	None	
		50	0.276	None	
2	Damage 1 (4–3)	−10	0.176	4–3 (0.674)	Damaged path detected
		20	0.262	4–3 (0.842)	
		50	0.285	4–3 (0.702)	
3	Damages 1 and 2 (4–3, 2–5)	−10	0.189	4–3 (0.693), 2–5 (0.923)	All damaged paths detected
		20	0.274	4–3 (0.778), 2–5 (0.875)	
		50	0.266	4–3 (0.725), 2–5 (0.926)	
4	Damages 1, 2 and 3 (2–4, 4–3, 1–5, 2–5)	−10	0.147	2–4 (0.375), 4–3 (0.647) 1–5 (0.807), 2–5 (0.921)	All damaged paths detected
		20	0.279	2–4 (0.339), 4–3 (0.737) 1–5 (0.841), 2–5 (0.862)	
		50	0.261	2–4 (0.508), 4–3 (0.663) 1–5 (0.764), 2–5 (0.930)	

6.2. Test results

The effect of a stiffener on Lamb wave propagation is investigated in Fig. 10. A toneburst signals is applied at PZT 1, and the corresponding Lamb wave responses are scanned over the rectangular area (80 mm × 150 mm) on the opposite side of what is shown in Fig. 10a using a scanning laser Doppler vibrometer (LDV). In Fig. 10b, it can be observed that the wavefront of the propagating

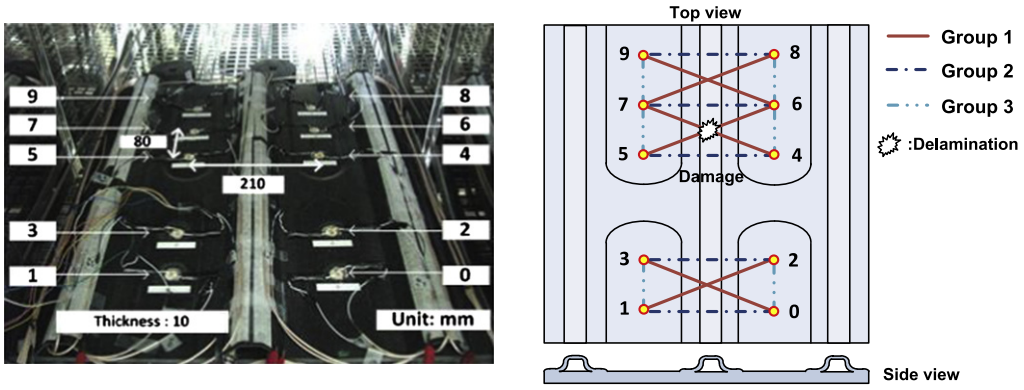

(a) A layout of the dual PZT network

(b) Damage location and wave propagation paths

Fig. 9. Configuration of a dual PZT network placed on a complex composite specimen with hat-shaped stiffeners. For the calculation of the DI in Eq. (2), pitch-catch signals are obtained from a total of the 17 paths, and they are divided into three groups having the same wave propagation distance.

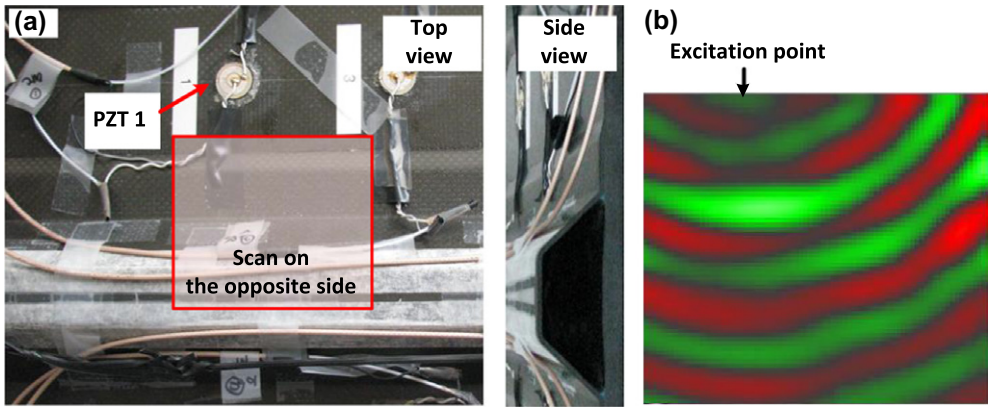

Fig. 10. Visualization of Lamb wave propagation near one of hat-shaped stiffeners using a Laser Doppler vibrometer: (a) scan area on the test specimen and (b) distortion of the wavefront due to the stiffener.

Table 2
Instantaneous diagnosis under changing temperatures (a complex composite plate).

Case	Damage location	Temp. (°C)	Threshold value	Damaged path(s) (DI value)	Damage diagnosis
1	No damage	−10	0.108	None	No damaged path detected
		20	0.147	None	
		50	0.202	None	
2	Damage (5–6, 4–7)	−10	0.227	5–6 (0.604), 4–7 (0.625)	Damaged path detected
		20	0.272	5–6 (0.639), 4–7 (0.699)	
		50	0.332	5–6 (0.717), 4–7 (0.761)	

Lamb waves are disturbed near the stiffener. The localization and extend of damage are only qualitatively estimated using a laser ultrasonic imaging technique developed by our research group [32,33].

The test results are summarized in Table 2. Similar to the previous experiment, no false-positive alarm is produced for the intact case (Case 1) and the two damaged paths crossing the delamination are successfully identified for the damage case (Case 2).

7. Conclusion

In this study, a new reference-free delamination technique is developed so that delamination in a multilayer composite plate even with stiffeners and under temperature variation can be detected by comparing pitch-catch Lamb wave signals obtained from a piezoelectric transducer network rather than by comparing each signal with its own corresponding baseline signal obtained from the pristine condition. The effectiveness of the proposed technique is validated using test data obtained from multi-layer carbon reinforced polymer composite plates with and without stiffeners. All wave propagation paths passing through impact induced delaminations are successfully identified while no false-positive alarms are produced from the intact conditions.

It should be noted that the proposed technique best operates under the following assumptions: (1) all dual PZTs are identical in terms of their sizes and bonding conditions; (2) the driving frequency is selected so that only the S_0 and A_0 modes are excited; and (3) temperature variation over the specimen is negligible although temperature variation over time is allowed. Finally, the damage localization performance can be improved by adding more PZT transducers with in the PZT network because this denser PZT network the population of wave

propagation paths in each group and decreases the minimum detectable damage size.

Acknowledgements

This work is supported by the Boeing Company, the Radiation Technology Program (M20703000015-07N0300-01510) and the Nuclear Research & Development Program (2009-0083489) of National Research Foundation of Korea (NRF) funded by Ministry of Education, Science & Technology (MEST).

Appendix A. A theoretical Lamb wave propagation model using circular PZTs

$$V(t) = C^{S_0}(t, r_s)S^{S_0}(a, c) + C^{A_0}(t, r_s)S^{A_0}(a, c) \tag{A.1}$$

where $C^{S_0}(t, r_s) = -i\dfrac{2\sqrt{2\pi}\tau_0 E_s h_s g_{31}}{\mu\sqrt{\xi^{S_0} r_s}} \dfrac{N_S(\xi^{S_0})}{D'_S(\xi^{S_0})} e^{i(\omega t - \frac{\pi}{4} + \xi^{S_0} r_s)}$,

$C^{A_0}(t, r_s) = -i\dfrac{2\sqrt{2\pi}\tau_0 E_s h_s g_{31}}{\mu\sqrt{\xi^{A_0} r_s}} \dfrac{N_A(\xi^{A_0})}{D'_A(\xi^{A_0})} e^{i(\omega t - \frac{\pi}{4} + \xi^{A_0} r_s)}$,

$S^{S_0}(a, c) = \dfrac{a}{c} J_1(\xi^{S_0} a) J_1(\xi^{S_0} c), \quad S^{A_0}(a, c) = \dfrac{a}{c} J_1(\xi^{A_0} a) J_1(\xi^{A_0} c).$

$$N_S(\xi) = \xi\beta(\xi^2 + \beta^2)\cos\alpha h \cos\beta h, \tag{A.2}$$

$N_S(\xi) = \xi\beta(\xi^2 + \beta^2)\sin\alpha h \sin\beta h,$

$D_S = (\xi^2 - \beta^2)^2 \cos\alpha h \sin\beta h + 4\xi^2\alpha\beta \sin\alpha h \cos\beta h$

$D_A = (\xi^2 - \beta^2)^2 \sin\alpha h \cos\beta h + 4\xi^2\alpha\beta \cos\alpha h \sin\beta h$

where $\alpha^2 = \dfrac{\omega^2}{c_L^2} - \xi^2, \quad \beta^2 = \dfrac{\omega^2}{c_T^2} - \xi^2, \quad c_L = \sqrt{\dfrac{\lambda + 2\mu}{\rho}}, \quad c_T = \sqrt{\dfrac{\mu}{\rho}}.$

Eq. (A.1) shows the output voltage response with respect to time t in the circular sensing PZT with a radius of c when a circular PZT with a radius of a is used as actuator. The first and second terms in Eq. (A.1) indicate the S_0 and A_0 modes, respectively. The spacing between exciting and sensing PZTs is r_s. The harmonic input signal exerted by the excitation PZT is modeled as 'pin-force model' that only produces surface shear stress τ_0 around its circumference boundary. E_s, h_s and g_s are Young's modulus, thickness and piezoelectric voltage constant of the sensing PZT, respectively. The ξ with superscript S_0 or A_0 is a wavenumber of S_0 or A_0 mode at a given input frequency ω. $N_s(\xi^{S_0})$, $D'_S(\xi^{S_0})$, $N_A(\xi^{A_0})$, and $D'_A(\xi^{A_0})$ in Eq. (A.1) can be computed using Eq. (A.2). λ and μ are Lame constants for the plate material, and ρ and h are the material density and thickness of the plate, respectively. $J_1()$ is the Bessel function of the first kind of order 1.

References

[1] Raghavan A, Cesnik CES. Review of guided-wave structural health monitoring. Shock Vib Dig 2007;39:91–114.
[2] Kessler SS, Spearing SM, Soutis C. Damage detection in composite materials using Lamb wave methods. Smart Mater Struct 2002;11:269–78.
[3] Giurgiutiu V, Cuc A. Embedded non-destructive evaluation for structural health monitoring, damage detection, and failure prediction. Shock Vib Dig 2005;37:83–105.
[4] Su Z, Ye L, Lu Y. Guided Lamb waves for identification of damage in composite structures: a review. J Sound Vib 2006;295:753–80.
[5] Frieden J, Cugnoni J, Botsis J, Gmür T. Low energy impact damage monitoring of composites using dynamic strain signals from FBG sensors – Part I: Impact detection and localization. Compos Struct 2012;94(2):438–45.
[6] Kirkby E, de Oliver R, Michaud V, Månson JA. Impact localisation with FBG for a self-healing carbon fibre composite structure. Compos Struct 2011;94(1):8–14.
[7] Takeda S, Aoki Y, Nagao Y. Damage monitoring of CFRP stiffened panels under compressive load using FBG sensors. Compos Struct 2012;94(3):813–9.
[8] Scalea FL, Salamone S. Temperature effects in ultrasonic Lamb wave structural health monitoring systems. J Acoust Soc Am 2008;124:161–74.
[9] Lu Y, Michaels JE. A methodology for structural health monitoring with diffuse ultrasonic waves in the presence of temperature variations. Ultrasonics 2005;43:717–31.
[10] Ip KH, Mai YW. Delamination detection in smart composite beams using Lamb waves. Smart Mater Struct 2004;13:544–51.
[11] Yang M, Qiao P. Modeling and experimental detection of damage in various materials using the pulse-echo method and piezoelectric sensors/actuators. Smart Mater Struct 2005;14:1083–100.
[12] Lestari W, Qiao P. Application of wave propagation analysis for damage identification in composite laminated beams. J Comp Mater 2005;39:1967–84.
[13] Toyama N, Noda J, Okabe T. Quantitative damage detection in cross-ply laminates using Lamb wave method. Compos Sci Technol 2003;63:1473–9.
[14] Guo N, Cawley P. The interaction of Lamb waves with delaminations in composite laminates. J Acoust Soc Am 1993;94:2240–6.
[15] Petculescu G, Krishnaswamy S, Achenbach JD. Group delay measurements using modally selective Lamb wave transducers for detection and sizing of delaminations in composites. Smart Mater Struct 2007;17:015007.
[16] Ihn JB, Chang FK. Pitch-catch active sensing methods in structural health monitoring for aircraft structures. Struct Health Monit 2008;7:5–19.
[17] Wang D, Ye L, Lu Y, Su Z. Probability of the presence of damage estimated from an active sensor network in a composite panel of multiple stiffeners. Comp Sci Technol 2009;69:2054–63.
[18] Yu L, Giurgiutiu V. In situ 2-D piezoelectric wafer active sensors arrays for guided wave damage detection. Ultrasonics 2008;48:117–34.
[19] Yan F, Rose JL. Guided wave phased array beam steering in composite plates, health monitoring of structural and biological systems. Proc SPIE 2007;6532:65320Gpp.
[20] Kim SB, Sohn H. Instantaneous reference-free crack detection based on polarization characteristics of piezoelectric materials. Smart Mater Struct 2007;16:2375–87.
[21] Ruzzene M, Xu B, Lee SJ, Michaels TE, Michaels JE. Damage visualization via beamforming of frequency–wavenumber filtered wavefield data. Proc SPIE 2010;7650:76500Lpp.
[22] Sohn H, Kim SB. Development of dual PZT transducers for reference-free crack detection in thin plate structures. IEEE Trans Ultrason Ferroelectr Freq Control 2010;57:229–40.
[23] Anton SR, Inman DJ. Reference-free damage detection using instantaneous baseline measurements. AIAA 2009;47:1952–64.
[24] Yeum CM, Sohn H, Ihn JB. Lamb wave mode decomposition using concentric ring and circular piezoelectric transducers. Wave Motion 2010;48:358–70.
[25] http://www.metisdesign.com (accessed 15.6.11).
[26] Hong JC, Sun KH, Kim YY. The matching pursuit approach based on the modulated Gaussian pulse for efficient guided wave damage detection. Smart Mater Struct 2005;14:548–60.
[27] Mallat SG, Zhang Z. Matching pursuits with time-frequency dictionaries. IEEE Trans Sig Proc 1993;41(12):3397–415.
[28] Xu B, Yu L, Giurgiutiu V. Advanced methods for time-of-flight estimation with application to lamb wave structural health monitoring. In: The 7th international workshop on structural health monitoring, Stanford, CA; 9–11 September 2009.
[29] Sohn H. Effect of environmental and operational variability on structural health monitoring. Proc Roy Soc A—Math Phys 2006;365:539–60.
[30] Deemer WL, Votaw DF. Estimation of parameters of truncated or censored exponential distributions. Ann. Math Stat 1955;26:498–504.
[31] Ross SM. Introduction to probability and statistics for engineers and scientists. 3rd ed. Academic Press; 2004. p. 504–8.
[32] Sohn H, Dutta D, Yang JY, Park HJ, DeSimio MP, Olson SE, et al. Delamination detection in composites through guided wave field image processing. Compos Sci Technol 2011;71:1250–6.
[33] Sohn H, Dutta D, Yang JY, DeSimio MP, Olson SE, Swenson ED. Automated detection of delamination and disbond from wavefield images obtained using scanning laser vibrometer. Smart Mater Struct 2011;20(4):045107.